Journal of Power Sources 245 (2014) 752–757

Contents lists available at SciVerse ScienceDirect

Journal of Power Sources

journal homepage: www.elsevier.com/locate/jpowsour

Study of an intermediate temperature solid oxide fuel cell sealing glass system

Kathy Lu*, Wenle Li [1]

Department of Materials Science and Engineering, Virginia Tech, Blacksburg, VA 24061, USA

HIGHLIGHTS

- A new sealing glass system is developed based on $SrO-La_2O_3-Al_2O_3-B_2O_3-SiO_2$.
- Atomic level microstructures and thermophysical characteristics are correlated.
- The most promising glass composition for solid oxide fuel cells is determined.

ARTICLE INFO

Article history:
Received 18 March 2013
Received in revised form
31 May 2013
Accepted 1 July 2013
Available online 13 July 2013

Keywords:
Sealing glass
Thermal expansion coefficient
Glass transition temperature
Glass network
Thermal stability

ABSTRACT

This study investigates the effect of composition on the atomic level structure and thermal characteristics of sealing glass for solid oxide fuel cells (SOFCs). The glass systems studied contain varying percentages of SiO_2, Al_2O_3, SrO, La_2O_3, and B_2O_3; and the composition variables examined are SrO and B_2O_3. Atomic level parameters, including boron coordination number with silicon, the probability of boron coordination with silicon, and glass network connectivity are calculated. Thermal expansion coefficients, glass softening temperatures, and glass transition temperatures are measured by dilatometry. The glasses are then thermally treated at 700 °C for up to 1500 h in order to study their long term thermal stability at SOFC operating conditions. The resulting data show that the most desired glass composition is stable for at least 1500 h without devitrification and is a very promising sealant for solid oxide fuel cells.

1. Introduction

Solid oxide fuel cells (SOFCs) are an exciting prospect in the energy world due to their ability to cleanly generate electricity through the use of hydrogen or syngas fuels with high efficiency. Typically, SOFCs operate at temperatures of 800 °C and higher. However, stringent material requirements demand lower operating temperatures in order to ease cell degradation problems during cell operation [1,2].

In order to keep the fuels and air in a cell stack from mixing or leaking, a sealant material must withstand the cell operating temperatures and repeated cycles without cracking and without reacting with other cell components. This means sealing materials that have the desirable thermophysical properties (thermal expansion coefficient, glass transition temperature, and glass softening temperature) and thermal stability are a must. To be used as a seal, glass should meet a combination of several requirements [3–5]. Glass transition temperature T_g should be high enough but less than cell operating temperature; for intermediate temperature SOFC use, this temperature is around 700 °C. Glass softening temperature T_s should be reasonably low, such as less than 1000 °C. The glass transition and softening temperatures are critical for proper fuel cell operation because of the cell dependence on the glass to relieve thermal stress and avoid cracks during cell operation [6–8] while still being viscous enough to seal the SOFC components. Glass coefficient of thermal expansion (CTE) should be greater than 8.0×10^{-6} K^{-1} to match with the CTEs of other cell components, which often include yttria stabilized zirconia, metallic interconnect, and lanthanum manganite electrode. More importantly, glass should not devitrify at SOFC operating temperatures for a long time (such as >40,000 h) in order to ensure cell stack durability.

BaO-containing aluminoborosilicate glass is the most common seal glass due to its excellent thermal properties [9–11]. This glass contains 35 mol% SiO_2, 10 mol% B_2O_3, 5.0 mol% Al_2O_3, 15 mol% CaO,

* Corresponding author. 211B Holden Hall, Materials Science and Engineering Department, Virginia Tech, Blacksburg, VA 24061, USA. Tel.: +1 540 231 3225; fax: +1 540 231 8919.
E-mail addresses: klu@vt.edu (K. Lu), wenle@vt.edu (W. Li).
[1] 127 Randolph Hall, Materials Science and Engineering Department, Virginia Tech, Blacksburg, VA 24061, USA. Tel.: +1 540 266 8020; fax: +1 540 231 5022.

0378-7753/$ – see front matter © 2013 Elsevier B.V. All rights reserved.
http://dx.doi.org/10.1016/j.jpowsour.2013.07.035

and 35 mol% BaO. The CTE of this glass is 11.8×10^{-6} K^{-1}; the T_g is intermediate, ~630 °C. This glass is often used at >800 °C and is attractive mainly because of its high CTE. However, there are two major drawbacks for this system. First, it crystallizes at 800 °C, forming celsian ($BaAl_2Si_2O_8$) and its polymorph hexacelcian phases [10]. Both these phases have low CTEs. Also, the difference in the CTE values of the celsian phase (2.29×10^{-6} K^{-1}) and the hexacelcian phase (8.0×10^{-6} K^{-1}) develops thermal stress and degrades cell performance [12]. Second, the glasses based on this system interact severely with chromium-containing steel interconnect and other fuel cell components [13]. The most detrimental reaction product is $BaCrO_4$, which has a CTE of 22×10^{-6} K^{-1}. Poor thermal and chemical stabilities of the BaO-containing aluminoborosilicate glass prompt the need to search for new BaO-free glass systems.

Another system is the SCAN2 glass reported by Smeacetto et al. [14], which contains 40 mol% SiO_2, 10 mol% B_2O_3, 9.0 mol% Al_2O_3, 18 mol% CaO, and 23 mol% Na_2O. The CTE is 11.2×10^{-6} K^{-1}; the T_g is ~545 °C. This is a low temperature seal glass for SOFCs with desirable CTE. However, it devitrifies extensively after thermal treatment at cell operating temperatures. The joining process with other cell components at 900 °C causes partial surface devitrification of the glass, resulting in a glass–ceramic seal.

A new glass system based on $SrO–La_2O_3–Al_2O_3–B_2O_3–SiO_2$ has been developed by us and possess excellent thermophysical properties and compatibility with other cell components [15–21]. It is a very desirable glass system for SOFC systems because of its high enough CTE (>10×10^{-6} K^{-1}) and superb devitrification resistance (stable for at least 2000 h at 800 °C). However, our previous efforts were mainly focused on 800 °C cell operating conditions. Therefore, the glass designs and thermophysical characterization were aimed for seal use at high temperatures. With the continuing efforts to decrease SOFC operating temperatures, there is a need to design new glass compositions for this glass system and re-examine the thermophysical characteristics and stability at lower temperatures.

In this work, $SrO–La_2O_3–Al_2O_3–B_2O_3–SiO_2$ glasses with different compositions are synthesized with the aim for a sealing system to be used at 700 °C. The glass atomic level bonding is calculated. The connectivity of the glass network and its relationship with the corresponding glass stability are discussed. The glass transition temperatures, softening temperatures, and CTEs are measured in order to characterize the thermophysical properties of the glass systems. Based on the above results, different promising glass samples are thermally treated at 700 °C for up to 1500 h. The most promising glass composition is identified.

2. Experimental procedure

Glass samples were prepared with conventional glass manufacturing process. $SrCO_3$ (99.9%, Sigma Aldrich, St. Louis, MO), La_2O_3 (99.98%), Al_2O_3 (99.95%), SiO_2 (99.8%), and B_2O_3 (99.98%) (All oxides were from Alfa Aesar, Ward Hill, MA) at designed compositions were mixed in a ball mill for overnight. The mixed oxides and carbonate were melted in a platinum crucible in a box furnace (Lindberg, Model No. 51314, Watertown, WI) at 1400 °C for 4 h. The heating schedule was at 10 °C min^{-1} heating rate from room temperature to 1100 °C; dwelling at 1100 °C for 1 h (for $SrCO_3$ to completely decompose); then heating at 5 °C min^{-1} to 1400 °C. Once the sample was sufficiently melted, it was poured into a graphite mold and all the excessive glass was poured into a bucket of water. The as-made glass samples were heated to 700 °C in a box furnace (Barnstead/Thermolyne Small Benchtop Muffle Furnace, 1400 Type). The samples were thermally treated at 700 °C for 1500 h in order to examine their thermal stability behaviors.

The glass samples were also cut with a diamond saw to about 25 mm long. The cylindrical glass sample end surfaces were polished with polishing papers and then different size alumina particle suspensions to optical finish (5 μm, 1 μm, 0.3 μm, and 0.05 μm) with flat, parallel ends. The flat ends were to ensure proper measurement of the thermal properties of the sealing glass. The glass transition temperature T_g, glass softening temperature T_s, and CTE were obtained by dilatometry (Orton Dilatometer Model 1000D, The Edward Orton Jr. Ceramic Foundation, Westerville, OH); the heating and cooling rates were 2.5 °C min^{-1}; the peak temperature was ~20 °C after glass softening temperature T_s, depending on the glass composition. The devitrification resistance analysis for different glass samples was carried out by X-ray diffraction (XRD, X'Pert PRO diffractometer, PANalytical B.V., EA Almelo, The Netherlands); the scan speed was 0.02°s^{-1} with Cu Kα radiation (λ = 1.5406 Å). A Raman spectrometer (JY Horbia LabRam HR 800, Horiba Ltd., Japan) was used to study the glass network structural stability. The Raman spectra were collected on polished glass samples in the range from 200 cm^{-1} to 1600 cm^{-1}, with a 514.57 nm argon laser light source at 50 mW power and 400 s exposure time. Afterward, the Raman spectra were deconvoluted using a GRAMS/AI_7.02 software (Themo Fisher Scientific, Inc. Waltham, MA). The details of Raman spectrum measurements were reported in our previous work [22].

3. Results

3.1. Sealing glass design principles

As explained in the Introduction section, in our prior studies, glasses based on the $SrO–La_2O_3–Al_2O_3–B_2O_3–SiO_2$ system were investigated as sealant for SOFCs [22,23]. The study shows that as the B_2O_3:SiO_2 ratio increases, the $SrO–La_2O_3–Al_2O_3–B_2O_3–SiO_2$ glass micro-heterogeneity and the amount of non-bridging oxygen atoms increase. Correspondingly, the T_g of the $SrO–La_2O_3–Al_2O_3–B_2O_3–SiO_2$ glasses changes from 635 °C to 775 °C and the T_d changes from 670 °C to 815 °C. Glass thermal stability decreases with B_2O_3:SiO_2 ratio increase. As a result, even though the glass without B_2O_3 is thermally stable after being kept at 800 °C for 2000 h, the lower temperature thermal behaviors of the glass system have not been studied since the focus of the prior study was to find a suitable sealing glass system for cells operating at 800 °C.

Based on our prior work, B_2O_3 is a necessary component for lowering the operating temperatures of the sealing glass. In this study, Al_2O_3 and La_2O_3 are kept constant during our new glass composition design. Different SrO levels are studied. The relative contents between SiO_2 and B_2O_3 are changed so that the effect of glass network formers can be analyzed while the total amount of SiO_2 and B_2O_3 stays the same at a given SrO level. When the B_2O_3 content is increased, the SiO_2 content is decreased by the same amount.

Because of the configurational entropy difference between SiO_4 and BO_3 structural units, SiO_4 structural units should preferentially link with BO_4 instead of BO_3 structural units, in addition to the bonding among SiO_4 themselves. To understand the degree of bonding between SiO_4 and BO_4 units in the designed glass systems, two related parameters can be calculated: probability of silicon coordinated to BO_4 and mean number of silicon coordinated to BO_4. Taking X_{Si} as the molar ratio of silicon to total network formers (silicon and boron) and assuming no BO_4 units are linked with each other, the mean number of silicon coordinated to BO_4 $\langle l \rangle$ can be expressed as [24]:

$$\langle l \rangle = \frac{16X_{Si}}{0.62 + 4.38X_{Si} - X_{Si}^2} \quad (1)$$

The probability of silicon coordinated to BO_4 $P(l)$ becomes:

$$P(l) = \frac{4!}{l!(4-l)!}\left(\frac{4X_{Si}}{0.62+4.38X_{Si}-X_{Si}^2}\right)^{l}\left(\frac{0.62+0.38X_{Si}-X_{Si}^2}{0.62+4.38X_{Si}-X_{Si}^2}\right)^{4-l} \quad (2)$$

Based on Equations (1) and (2), $<l>$ and $P(l)$ can be calculated for the glasses as shown in Fig. 1. $<l>$ and $P(l)$ decrease constantly with B_2O_3 content increase.

For the 20 mol% SrO glass series (Fig. 1a), understandably $<l>$ and $P(l)$ are zero at 0 mol% B_2O_3 content since no SiO_4 can be bonded to BO_4. At 5 mol% B_2O_3 content, the mean number of silicon coordinated to BO_4, $<l>$, is 3.78; the probability of finding silicon coordinated to BO_4, $P(l)$, is 0.80, the highest values in this glass series. When the B_2O_3 content increases to 10 mol%, there is a decrease in $<l>$ and $P(l)$; they are 3.59 and 0.65, respectively. When the B_2O_3 content is increased to 15 mol% and higher, $<l>$ decreases to 3.41 and $P(l)$ drastically decreases to 0.40 or lower. This means that as the B_2O_3 content increases, there are not only fewer silicon atoms coordinated to BO_4 standard units but also the possibility of finding such coordination drastically decreases. Put it differently, SiO_4 and BO_4 structural units are less likely to bond with each other with B_2O_3 content increase, even by assuming that no BO_4 units are directly linked with themselves. For the 20 mol% SrO glass series as well as the other two glass series to be discussed later, the drastic decreases in $<l>$ and $P(l)$ occur at 15 mol% B_2O_3 content. This indicates that glass thermophysical properties should be considered jointly with the glass structural unit distribution and bonding when evaluating a glass system.

For the 25 mol% SrO glass series, very similar observations can be made (Fig. 1b). Initially, both $<l>$ and $P(l)$ are zero at 0 mol% B_2O_3 content. As 5 mol% B_2O_3 is introduced into the system, there is a high tendency for BO_4 and SiO_4 to be coordinated; the $<l>$ and $P(l)$ values are 3.77 and 0.94, respectively. However, when the B_2O_3 content increases to 10 mol%, $<l>$ and $P(l)$ decrease to 3.56 and 0.89, respectively. For 15 mol% and higher B_2O_3 content conditions, $<l>$ and $P(l)$ drastically decrease to lower than 3.40 and 0.30, respectively.

For the 30 mol% SrO glass series (Fig. 1c), the trends and the $<l>$ and $P(l)$ values are very similar to those of the 25 mol% SrO glass series and will not be elaborated here. However, it should be pointed out that at low B_2O_3 contents (5 and 10 mol%), high SrO levels (25 mol% and 30 mol%) have no significant impact on the SiO_4 and BO_4 coordination probability while lower SrO level (20 mol%) significantly decreases it. This is likely due to the more extensive interaction between the SiO_4 and BO_4 structural units with less presence of SrO. However, when the B_2O_3 content increases to 15 and 20 mol%, the SiO_4 and BO_4 coordination probability decreases to a larger extent at higher SrO levels (25 and 30 mol%). This is likely due to the low presence of SiO_4 structural units in general. Apparently, both SrO and B_2O_3 changes have significant impact on the glass atomic level bonding.

3.2. Thermophysical characteristics

Even though the glass atomic level bonding calculation provides useful data on the sealing glass structural changes and glass stability tendency and serves as a good guide on glass composition design, it does not provide information on the glass thermophysical behaviors (glass transition temperature T_g, glass softening temperature T_s, and CTE) that are critical for the sealing use. Dilatometry data are thus examined in order to evaluate the suitability of the studied glass compositions for SOFC use. As shown in Fig. 2, both the glass transition temperature and softening temperature decrease consistently with the increase of the B_2O_3 content, at all SrO composition levels. The decreases in the glass transition and softening temperatures with B_2O_3 content increase are expected.

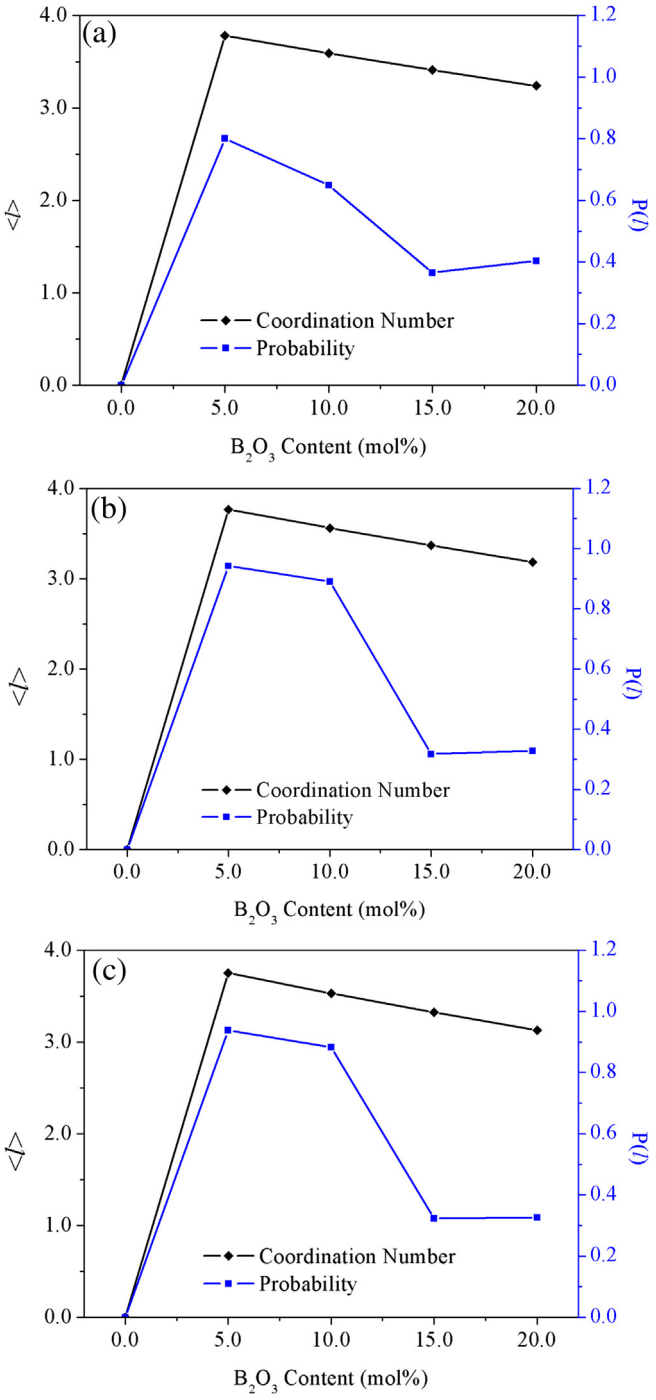

Fig. 1. Mean number of silicon coordinated to BO_4 $<l>$ and probability of silicon coordinated to BO_4 $P(l)$ at different SrO content: (a) 20 mol% SrO, (b) 25 mol% SrO, and (c) 30 mol% SrO.

This is not only because borate glasses are known for low T_g and T_d, but also because trigonal BO_3 polyhedrals contributed by B_2O_3 addition lead to rearrangement of the rigid SiO_4 glass network and result in much mobile network structures. CTEs, on the other hand, show very inconsistent trends and cannot be correlated with the B_2O_3 content increase. This finding indicates that CTE of glasses does not follow simple additive rules based on compositions, which has been attempted in the literature [25–28]. The thermal expansion behavior of glass involves complex interactions at atomic level bonding and the changes of species behaviors with composition variation.

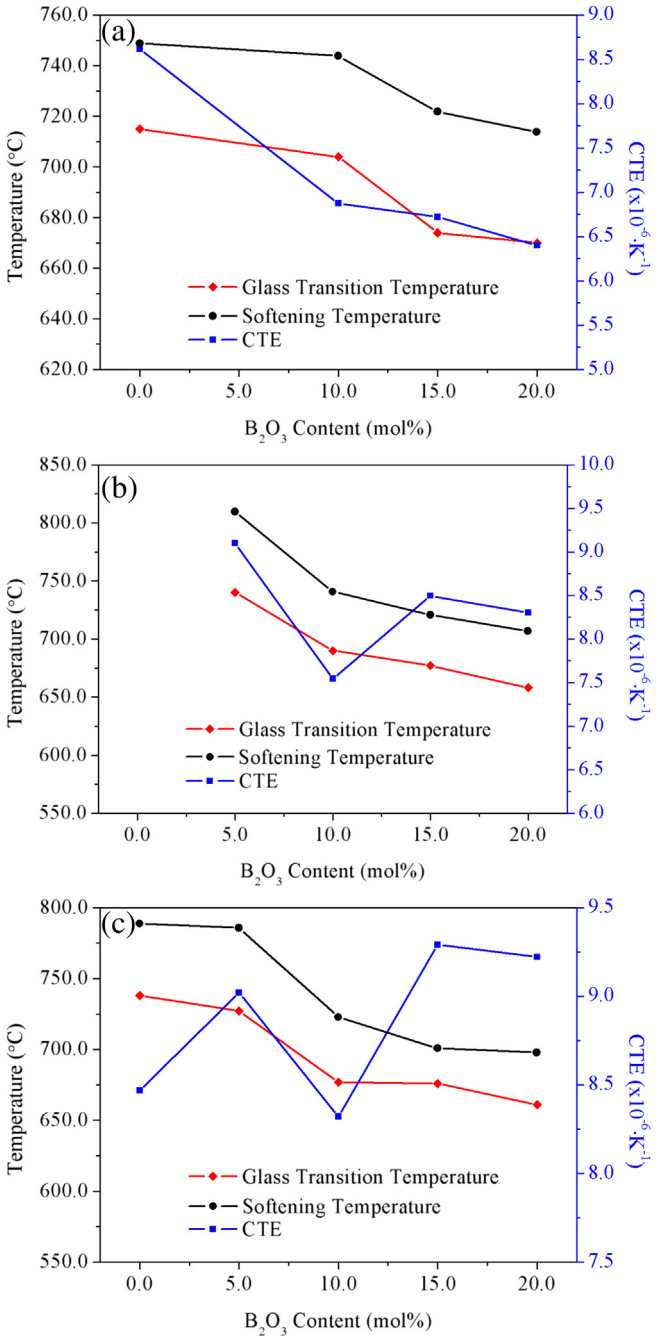

Fig. 2. Glass transition temperature, glass softening temperature, and CTE at different B_2O_3 content: (a) 20 mol% SrO, (b) 25 mol% SrO, and (c) 30 mol% SrO.

Nonetheless, useful results can be obtained from Fig. 2 based on T_g, T_s, and CTE. First, for the 20 mol% SrO glass series, the T_g of the 0 mol% B_2O_3 glass sample is too high (715 °C) for intended 700 °C use, which dictates that the T_g must be lower than 700 °C. The 5 mol % B_2O_3 glass sample cannot be made into 25 mm long rod for the dilatometry test because of the very high viscosity of the glass at the 1400 °C melting state, which also indicates unsuitable T_g for the intended use. This is why the data points are absent for this glass composition in Fig. 2a. Even though the remaining glass compositions have low T_g, the CTE for each glass composition is too low ($<7.0 \times 10^{-6}\,K^{-1}$). These glass compositions are deemed unsuitable for sealing purposes.

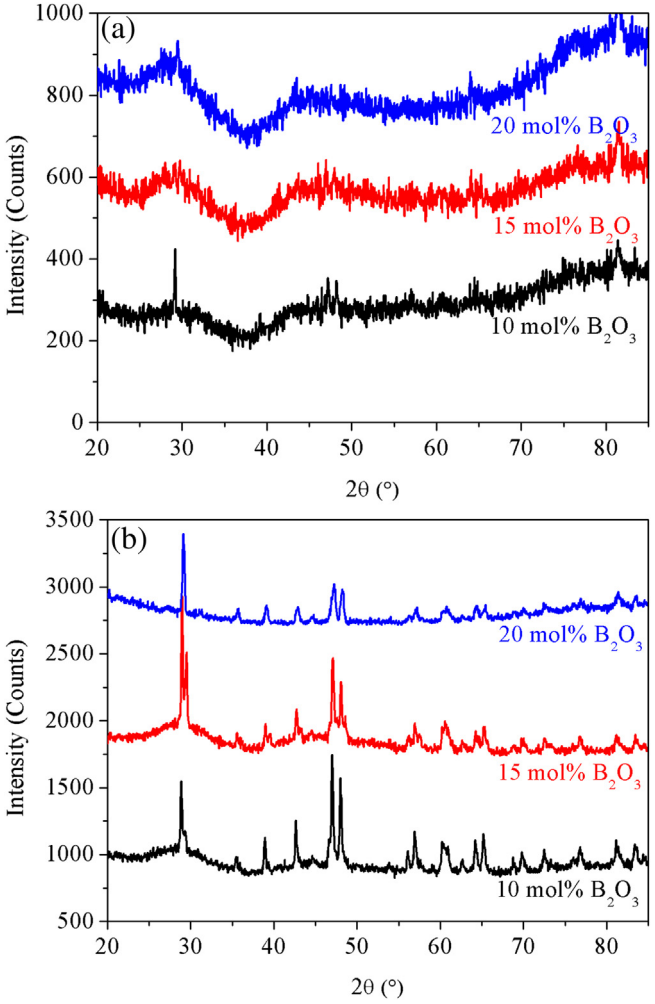

Fig. 3. X-ray diffraction patterns of as-synthesized glass samples at different B_2O_3 contents. (a) 25 mol% SrO, (b) 30 mol% SrO.

For the glass series with 25 mol% SrO content (Fig. 2b), the data for the 0 mol% B_2O_3 glass sample are omitted since the glass devitrification resistance is too low and extensive devitrification occurs during the glass synthesis. For the 5 mol% B_2O_3 content, the T_g is too high at 740 °C. For the remaining glass compositions (10, 15, and 20 mol% B_2O_3), the T_s values are above 700 °C (741 °C, 721 °C, and 707 °C, respectively, at 10, 15, and 20 mol% B_2O_3), the T_g is below 700 °C (at 690 °C, 677 °C, and 658 °C, respectively at 10, 15, and 20 mol% B_2O_3). The CTEs at high B_2O_3 compositions are $8.50 \times 10^{-6}\,K^{-1}$ and $8.30 \times 10^{-6}\,K^{-1}$, respectively, for 15 and 20 mol % compositions. This is at the low end of the desired CTE values. However, the studied sealing glass here is also meant for intermediate temperature SOFCs (~700 °C). The thermal stress and the temperature cycling condition are less severe. So such CTE values should still work.

For the 10 mol% B_2O_3 composition, the CTE is on the low side ($7.54 \times 10^{-6}\,K^{-1}$) but is included for further studies. As pointed out before, the irregular CTE changes cannot be explained based on composition variation and remains one of the most puzzling aspects for sealing glass design.

For the glass with 30 mol% SrO content (Fig. 2c), the T_g is too high at ≤5 mol% B_2O_3 content (738 °C and 727 °C for 0 and 5 mol% B_2O_3 contents, respectively). For the remaining glass compositions (10, 15, and 20 mol% B_2O_3), T_g and CTE are in the desirable ranges

Table 1
Glass network connectivity and related parameters.

B_2O_3 content, SrO is kept at 25 mol%	Total bond strength $\left[\frac{\sum_i Z_i(F_iV_i)}{\sum_i Z_iV_i}\right]_{\text{Network Former}}$ $\left[\frac{\sum F_iV_i}{\sum V_i}\right]_{\text{Network Former+Modifier}}$	Ratio of bridging oxygens vs. total oxygens $\frac{\sum O^+}{\sum O^- + \sum O^+}$	Connectivity ψ
10 mol%	1.2445	0.4271	0.5315
15 mol%	1.2336	0.6664	0.8221
20 mol%	1.2234	0.4695	0.5744

($T_g < 700$ °C, CTE $> 8.0 \times 10^{-6}$ K^{-1}) even though the T_s is 698 °C for the 20 mol% B_2O_3 glass sample, lower than desired. Especially, the latter two glass systems (15 and 20 mol% B_2O_3) worth further examination because of the $>9.2 \times 10^{-6}$ K^{-1} CTEs.

3.3. Devitrification resistance

Besides glass atomic level bonding and thermophysical properties, the third critical requirement for sealing glass is devitrification resistance. For the remaining promising glass compositions, which include 10–20 mol% B_2O_3 contents at 25 and 30 mol% SrO levels, the as-synthesized glass XRD patterns are given in Fig. 3. The glasses with 25% SrO are mostly amorphous. For the glass with 10 mol% B_2O_3, the XRD pattern has a peak around 27°. There are also a couple of very weak peaks in the 80–85° 2θ range for all these three glass formulas. While individual peaks appear in the samples, which is a sign of small portions of crystalline phases, none of these crystalline phases are fully developed and therefore no specific phases can be detected.

When the SrO content is at 30 mol%, Fig. 3b shows clear devitrification for the glass series. The crystalline phases include $Sr_3B_2O_6$, $LaBO_3$, and $La_2Si_2O_7$. The glasses with 30 mol% SrO have higher amounts of crystallized phases than the samples with 25 mol% SrO (Fig. 3a). The 30 mol% SrO glass series is deemed unsuitable as sealing glasses because of the extensive devitrification.

For the three remaining most promising sealing glass compositions at 25 mol% SrO level, the glass network structural stability can be examined by considering the bonding strength and bridging/non-bridging oxygens in the system. It is generally assumed that non-bridging oxygen species (SrO and La_2O_3) decrease glass connectivity. The local ordering of the glass structural units increases micro-heterogeneity and configurational entropy and decreases the system free energy [29]. The devitrification tendency of glass increases if many glass structure units are present and have a tendency

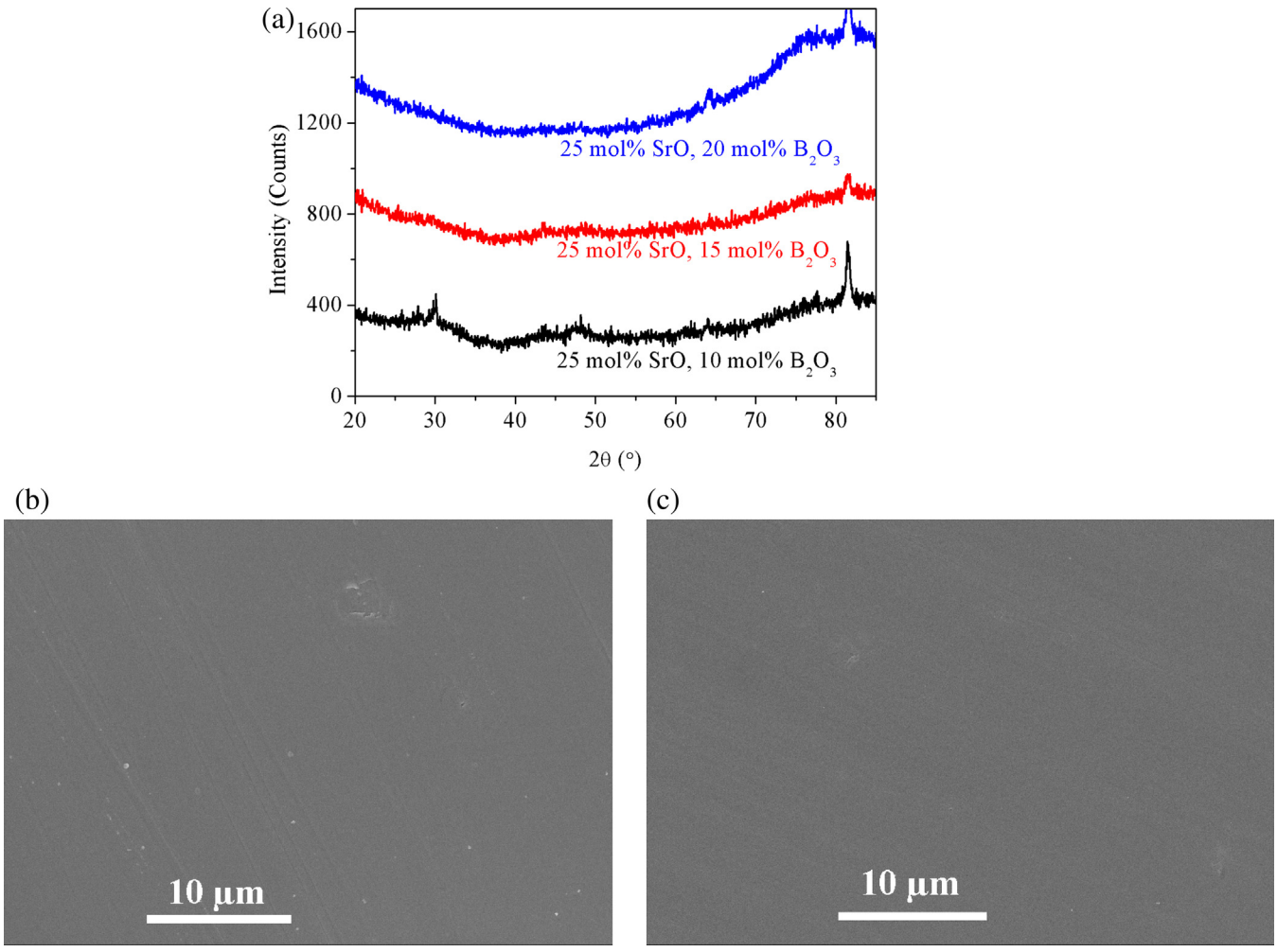

Fig. 4. The 25 mol% SrO glass samples thermally treated at 700 °C for 1500 h: (a) XRD patterns, (b) SEM image of the 15 mol% B_2O_3 sample, (c) SEM image of the 20 mol% B_2O_3 sample.

to segregate. The glass stability is mainly determined by the glass network connectivity, which can be quantified by determining the non-bridging oxygen amount from Raman spectroscopy [22,23]:

$$\psi = \frac{\left[\frac{\sum Z_i(F_iV_i)}{\sum Z_iV_i}\right]_{\text{Network Former}}}{\left[\frac{\sum F_iV_i}{\sum V_i}\right]_{\text{Network Former+Modifier}}} \cdot \frac{\sum O^+}{\sum O^- + \sum O^+} \quad (3)$$

ψ is the degree of glass network connectivity, F_i is the field strength of oxide i in a glass system, V_i is the amount of oxide i in vol%, and Z_i is the atomic number of oxide i. The first term in Equation (3) considers the bonding effect of cations in a glass network and remains the same for the studied glass system. The second term represents the ratio of bridging oxygen atoms (O^+) vs. the total oxygen atoms (O^- and O^+) in a glass network. The three remaining glass compositions are only different in the relative amount of glass formers (SiO_2 and B_2O_3) that provide the backbone of the glass. Therefore, the glass network connectivity calculation should be fairly predictive. When more variables are involved, the predictability is compromised because of the complex interrelations between the compositions and network structures. For the 10, 15, and 20 mol% B_2O_3 content glasses at 25 mol% SrO level, the parameters for Equation (3) can be calculated as shown in Table 1.

Based on Table 1, it can be projected that the 15 mol% B_2O_3 glass composition should be most stable, followed by the 20 mol% B_2O_3 composition and then the 10 mol% B_2O_3 composition. However, the stability of the latter two should be fairly close. With this understanding, these three most promising glass samples are treated at 700 °C for 1500 h. The XRD and microstructure results for the thermally treated samples are given in Fig. 4. As it shows, in the 80–85° 2θ range there is a very small peak for the 15 mol% B_2O_3 glass sample but there are more visible peaks for the 10 and 20 mol% B_2O_3 content samples. The SEM images (Fig. 4b and c) show amorphous microstructures for both samples except for some small polishing debris in Fig. 4b. This observation is consistent with the calculation in Table 1 that shows lower glass network connectivity for the 10 and 20 mol% B_2O_3 compositions. Also, the small peak at 81° is present at the as-synthesized state for the 15 mol% B_2O_3 glass sample. The 1500 h thermal treatment does not lead to peak increase. This means the 15 mol% B_2O_3 glass is very stable at 700 °C. For the 10 and 20 mol% B_2O_3 samples, the emerging new phases are almost impossible to be indexed because of the limited number of peaks and the low intensities of some peaks. However, the possibilities are $La_2Si_2O_7$, $Sr_3B_2O_6$, $SrSiO_3$, and Al_2O_3. Regardless, the 15 mol% B_2O_3 sample has the most stable amorphous phase. In this study, the thermal treatment is discontinued because of the time constraint. Longer time thermal treatment will provide more details for the devitrification resistance and durability of the 15 mol% B_2O_3 glass composition when used in SOFC stacks.

4. Conclusions

This study is focused on developing a sealing glass system that has the desirable thermophysical characteristics to be used in SOFCs operating at 700 °C with long term devitrification resistance. The main variables examined are glass atomic level bonding characteristics, glass network connectivity, and thermophysical parameters (including glass transition temperature, glass softening temperature, and thermal expansion coefficient). More importantly, glass devitrification resistance has been evaluated by thermally treating promising glass samples at 700 °C for up to 1500 h. The most promising glass composition has 15 mol% B_2O_3 and 25 mol% SrO. The glass transition temperature for the glass is 677 °C; the glass softening temperature is 721 °C; and the thermal expansion coefficient is $8.5 \times 10^{-6}\,K^{-1}$. It also has much higher glass network connectivity of 0.82 vs. others at ~0.55. In addition, this glass is stable at 700 °C for at least 1500 h. Understanding of its long term thermal behaviors in actual SOFC stacks will answer the ultimate question about its suitability as a SOFC sealant.

Acknowledgments

The authors acknowledge the financial support from Institute for Critical Technology and Applied Science of Virginia Tech and Prof. Bob Bodnar's Group for the Raman Spectroscopy.

References

[1] Z.P. Shao, S.M. Haile, Nature 431 (2004) 170–173.
[2] D.J.L. Brett, A. Atkinson, N.P. Brandon, S.J. Skinner, Chem. Soc. Rev. 37 (2008) 1568–1578.
[3] K.S. Weil, J. Miner. Met. Mater. Soc. 58 (2006) 37–44.
[4] J.W. Fergus, J. Power Sources 147 (2005) 46–57.
[5] EG&G Technical Services, Fuel Cell Handbook, seventh ed., US Department of Energy, Office of Fossil Energy, National Energy Technology Laboratory, Morgantown, WV, 2004.
[6] H.D. Ackler, J. Am. Ceram. Soc. 81 (1998) 3093–3103.
[7] P. Hrma, W.T. Han, A.R. Cooper, J. Non-Cryst. Solids 102 (1988) 88–94.
[8] R.N. Singh, Int. J. Appl. Ceram. Technol. 4 (2007) 134–144.
[9] Z.G. Yang, J.W. Stevenson, K.D. Meinhardt, Solid State Ionics 160 (2003) 213–225.
[10] K.D. Meinhardt, D.S. Kim, Y.S. Chou, K.S. Weil, J. Power Sources 182 (2008) 188–196.
[11] Z.G. Yang, K.D. Meinhardt, J.W. Stevenson, J. Electrochem. Soc. 150 (2003) A1095–A1101.
[12] S.B. Sohn, S.Y. Choi, G.H. Kim, H.S. Song, G.D. Kim, J. Am. Ceram. Soc. 87 (2004) 254–260.
[13] Z.G. Yang, G.G. Xie, K.D. Meinhardt, K.S. Weil, J.W. Stevenson, J. Mater. Eng. Perform. 13 (2004) 327–334.
[14] F. Smeacetto, M. Salvo, A. Ferraris, V. Casalegno, P. Asinari, J. Eur. Ceram. Soc. 28 (2008) 611–616.
[15] M.K. Mahapatra, K. Lu, Fuel Cells 11 (2011) 436–444.
[16] M.K. Mahapatra, K. Lu, J. Power Sources 196 (2011) 700–708.
[17] M.K. Mahapatra, K. Lu, J. Power Sources 195 (2010) 7129–7139.
[18] M.K. Mahapatra, K. Lu, Int. J. Hydrogen Energy 35 (2010) 11908–11917.
[19] M.K. Mahapatra, K. Lu, W.T. Reynolds, J. Power Sources 179 (2008) 106–112.
[20] M.K. Mahapatra, K. Lu, Mater. Sci. Eng. R 67 (2010) 65–85.
[21] T. Jin, K. Lu, J. Power Sources 195 (2010) 4853–4864.
[22] M.K. Mahapatra, K. Lu, R.J. Bodnar, Appl. Phys. A 95 (2009) 493–500.
[23] K. Lu, M.K. Mahapatra, J. Appl. Phys. 104 (2008) 074910.
[24] L.S. Du, J.F. Stebbins, J. Phys. Chem. B 107 (2003) 10063–10076.
[25] H. Scholze, Glass – Nature, Structure and Properties, Springer-Verlag, New York, 1990.
[26] J.M. Stevels, Progress in the Theory of the Physical Properties of Glasses, Elsevier Pub. Co., New York, 1948.
[27] A.I. Priven, Glass Technol. 45 (2004) 244–254.
[28] K. Takahashi, J. Soc, Glass Technol. 37 (1953) 3N–7N.
[29] T. Maehara, T. Yano, S. Shibata, M. Yamane, Philos. Mag. 84 (2004) 3085–3099.